9B.6

Lagrangian Coherent Structures and Vortical Hot Towers

Blake Rutherford[1], Gerhard Dangelmayr[1], and Michael Montgomery[2]
[1]Department of Mathematics, Colorado State University, Fort Collins, CO 80523-1874
[2]Department of Meteorology, Naval Postgraduate School, Monterey, CA 93943-5114

May 6, 2010

1 Introduction

Tropical cyclogenesis is an inherently 3D and asymmetric process, marked by the spinup of individual moist convective mesovortices [20], which are found in the tropical atmosphere prior to the formation of a tropical depression. There are two proposed mechanisms for the spinup of TC's. The first is through sea-surface winds that transfer energy to the core through wind induced surface heat exchange (WISHE) [12]. The second mechanism is through the interaction of warm-core vortex structures, termed vortical hot towers (VHT's) [10]. The VHT's are assumed to be the key coherent structure present during TC formation [13, 1]. Their role for intensification is highly important, as the axisymmetric vortex does not develop until the temperature in the surrounding environment reaches the temperature in the VHT's. Thus, the thermal transport properties associated with the interaction of VHT's play a key role for intensification.

VHT's are localized structures creating a protected environment [11] which supports the conversion of latent heat into rotational energy [18, 4] during their lifecycle of approximately 1 hour. Though VHT's have a small horizontal scale, their upscale organization is a mechanism for the transport of energy into a single vortex [13]. Their relation to environmental flow is not well understood, although in [1] the low entrainment rate of cat's eye features is proposed as a potential mechanism for less disturbance from the environment. The studies of [2] and [3] provide some insight into the effects of environmental flow for mature storms, but the case of a developing storm is still not understood.

Understanding the transport induced by VHT interaction requires advanced mathematical techniques, due to the spatio-temporal complexities of the velocity fields. VHT's are the most obvious coherent structure during intensification, and are seen as regions of high convection and vorticity. They are also trackable, and robust through changing wind fields. However, their role in the transport of thermodynamic properties cannot be fully understood without knowledge of the related flow dividing structures associated with VHT's. The interaction between mesovortices can be characterized by the coherent structures between them, which either allow or prohibit interaction. The manifolds linking VHT's cannot be found by Eulerian methods, since it requires following trajectories. The time-dependence of the velocity fields implies that the manifolds are of finite length. The appearance of these connecting structures has been seen in Eulerian phase portraits, see e.g. [15, 1], but they are difficult to track and visualize due to the time-dependence and shear present in tropical cyclones.

A new class of finite-time Lagrangian methods allows for the detection of Lagrangian coherent structures (LCS's), which are the finite-time analog of stable and unstable manifolds.

Haller and coauthors [8, 9, 5] proposed finite-time Lyapunov exponents (FTLE's) as a method for measuring trajectory separation, and maximal ridges of an FTLE field mark LCS's. Though FTLE's are easily computed, and handle time-dependence and approximation errors of velocity data, they do not differentiate between hyperbolicity and shear effectively, and are therefore limited for atmospheric flows. The study of [17] showed that the methods of [7] could be used even in the presence of large-scale shear to detect LCS's.

The 2D method of separating shear was extended to 3D in [16], and was used to compute a Lagrangian eye-eyewall interface during a mature, but still highly time-dependent velocity field. In this study, 3D flow separation has been decomposed into several hyperbolic and shear components. Additional benefits of the method were that it offers faster convergence than FTLE's and handles the difficult aspect ratio present in tropical cyclones. The key ingredient in the approach of [16] was a specific choice of coordinates adapted to the helical trajectory motion. Though the VHT interaction is clearly more complex than the evolution of a single vortex, the coordinate system proposed in [16] is still valid, as long as trajectories entrained in vortices remain there over sufficiently long time periods.

In this study, we apply the methods of [16] to a 3D intensifying tropical cyclone, and examine the LCS's involved in VHT interaction. We show that while the VHT's constitute an important type of LCS, which is parabolic, the hyperbolic LCS's separating the VHT's are shown to control the transport of material into the core, and are thus the important LCS's involved in tropical cyclogenesis. Moreover, the hyperbolic structures cannot be isolated by the field of FTLE's. Our study also shows the length scales over which VHT's can interact, and demonstrates that multiple VHT's may be involved in this interaction [10], which may result in the upscale organization proposed by [13].

2 Preliminaries

Given a time-dependent velocity field $\mathbf{u}(\mathbf{x}, t)$, Lagrangian methods are based on the separation of trajectories $\mathbf{x}(t)$. The flow map after an integration time τ maps an initial point $\mathbf{x}(t_0)$ to $\mathbf{x}(t_0 + \tau)$. The class of Lagrangian trajectory based approaches determine finite-time transport through the separation of nearby trajectories [9, 6, 19]. Finite time Lyapunov exponents (FTLE's) have become a standard representation of this separation, and provide scalar fields which show manifolds as ridges. Computing the FTLE forward ($\tau > 0$) and backward ($\tau < 0$) in time allows detection of forward time repelling and attracting material lines, respectively.

While FTLE's are an efficient measure of trajectory separation, they do not differentiate between hyperbolicity and shear. However, this distinction can be made by solutions of the variational equation

$$\dot{\boldsymbol{\xi}} = \nabla\mathbf{u}(\mathbf{x}(t), t)\boldsymbol{\xi}. \tag{1}$$

The Lagrangian velocity direction is given by the unit tangent vector

$$\mathbf{t} = \frac{\mathbf{u}}{|\mathbf{u}|}, \tag{2}$$

evaluated along trajectories. A moving frame of reference for (1) is introduced along a trajectory by setting

$$\boldsymbol{\xi} = T(\mathbf{x}(t), t)\boldsymbol{\eta}, \tag{3}$$

where the columns of T are the unit vectors $\mathbf{t}, \mathbf{n}, \mathbf{b}$,

$$T(\mathbf{x}, t) = [\mathbf{t}(\mathbf{x}, t), \mathbf{n}(\mathbf{x}, t), \mathbf{b}(\mathbf{x}, t)], \tag{4}$$

which are assumed to form an orthonormal frame of reference along the trajectory. The unit normal $\mathbf{n}$ can be chosen as arbitrary unit normal vector in the normal plane, and the binormal $\mathbf{b}$ is given by $\mathbf{b} = \mathbf{t} \times \mathbf{n}$. A convenient choice for $\mathbf{n}$ is introduced below. The transformed system for $\boldsymbol{\eta}$ has the form

$$\dot{\boldsymbol{\eta}} = [A(\mathbf{x}(t), t) + B(\mathbf{x}(t), t)]\boldsymbol{\eta}, \tag{5}$$

where $A(\mathbf{x}, t) = T^*(\nabla \mathbf{u})T - T^*(T_{\mathbf{x}}\dot{\mathbf{x}})$ (asterisks denote transposed matrices or vectors) with

$$T_{\mathbf{x}}\dot{\mathbf{x}} = \big[(\nabla \mathbf{u})\mathbf{t} - [\mathbf{t}^*(\nabla \mathbf{u})\mathbf{t}]\mathbf{t}, (\nabla \mathbf{n})\mathbf{u}, (\nabla \mathbf{b})\mathbf{u}\big],$$

and $B(\mathbf{x}, t) = -[\mathbf{b}_1, T^*\mathbf{n}_t, T^*\mathbf{b}_t]$ with $\mathbf{b}_1 = (1/|\mathbf{u}|)\,[0, \mathbf{n}^*\mathbf{u}_t, \mathbf{b}^*\mathbf{u}_t]^*$ contains all terms of the transformed matrix that depend on the time derivatives of $\mathbf{u}, \mathbf{n}, \mathbf{b}$ (indicated by the subscript t), thus B vanishes in the case of autonomous velocity fields.

Combining the two terms of which A is composed yields $A = [\mathbf{a}_1, T^*\mathbf{a}_2, T^*\mathbf{a}_3]$, where

$$\begin{aligned} \mathbf{a}_1 &= [\mathbf{t}^*(\nabla \mathbf{u})\mathbf{t}, 0, 0]^*, \\ \mathbf{a}_2 &= (\nabla \mathbf{u})\mathbf{n} - (\nabla \mathbf{n})\mathbf{u}, \\ \mathbf{a}_3 &= (\nabla \mathbf{u})\mathbf{b} - (\nabla \mathbf{b})\mathbf{u}. \end{aligned}$$

As in our study of the 2D case [17], we assume that the time derivatives along trajectories are small and can be neglected. Thus we use the following approximation of the transformed variational system,

$$\dot{\boldsymbol{\eta}} = A(\mathbf{x}(t), t)\boldsymbol{\eta}. \tag{6}$$

2.1 Transformation to upper triangular form and solution of the variational system

In contrast to the 2D case, the matrix A is not upper triangular. To obtain upper triangular form we apply a time-dependent orthogonal transformation in the normal plane. The normal plane component, $\boldsymbol{\eta}^\perp = (\eta_2, \eta_3)^*$, satisfies $\dot{\boldsymbol{\eta}}^\perp = A^\perp \boldsymbol{\eta}$ with

$$A^\perp = \begin{pmatrix} A_{22} & A_{23} \\ A_{32} & A_{33} \end{pmatrix}. \tag{7}$$

Let $\phi(t)$ be a solution to the differential equation

$$\dot{\phi} = \frac{1}{2}(A_{33} - A_{22}) \sin 2\phi + A_{23} \sin^2 \phi - A_{32} \cos^2 \phi, \tag{8}$$

and $R(\phi)$ the rotation matrix

$$R(\phi) = \begin{pmatrix} \cos \phi & \sin \phi \\ -\sin \phi & \cos \phi \end{pmatrix}. \tag{9}$$

The transformation $\boldsymbol{\eta}^\perp = R(\phi(t))\widetilde{\boldsymbol{\eta}}^\perp$ transforms the normal plane system to

$$\dot{\widetilde{\boldsymbol{\eta}}}^\perp = \widetilde{A}^\perp \widetilde{\boldsymbol{\eta}}^\perp. \tag{10}$$

Thus, dropping the tilde, we may assume that A in (6) has the form

$$A(\mathbf{x}(t), t) = \begin{pmatrix} A_{11} & A_{12} & A_{13} \\ 0 & A_{22} & A_{23} \\ 0 & 0 & A_{33} \end{pmatrix}, \tag{11}$$

and the transformed variational system can be solved by direct integration. The fundamental matrix for the system (6) with A given by (11) is found by direct integration as

$$\Psi(t,t_0) = \begin{pmatrix} \Psi_{11}(t,t_0) & \Psi_{12}(t,t_0) & \Psi_{13}(t,t_0) \\ 0 & \Psi_{22}(t,t_0) & \Psi_{23}(t,t_0) \\ 0 & 0 & \Psi_{33}(t,t_0) \end{pmatrix}, \tag{12}$$

where the diagonal elements can be written as

$$\Psi_{ii}(t,t_0) = \exp\big(\int_{t_0}^{t} A_{ii}(\tau)\,d\tau\big),$$

and the off-diagonal elements as

$$\begin{aligned} \Psi_{12} &= \int_{t_0}^{t} \exp\left(\int_s^t A_{11}(\tau)\,d\tau\right)\exp\left(\int_{t_0}^{s} A_{22}(\tau)\,d\tau\right) A_{12}(s)\,ds, \\ \Psi_{23} &= \int_{t_0}^{t} \exp\left(\int_s^t A_{22}(\tau)\,d\tau\right)\exp\left(\int_{t_0}^{s} A_{33}(\tau)\,d\tau\right) A_{23}(s)\,ds, \\ \Psi_{13} &= \int_{t_0}^{t} \exp\left(\int_s^t A_{11}(\tau)\,\tau\right)\Big[\Psi_{23}(s,t_0)A_{12}(s) \quad + \exp\left(\int_{t_0}^{s} A_{33}(\tau)\,d\tau\right)A_{13}(s)\Big]\,ds. \end{aligned} \tag{13}$$

For a 3D hurricane, the motion in the eyewall can be described as helical, with rotational and vertical components.

2.1.1 Horizontally aligned normal vector

A convenient choice for the unit normal $\mathbf{n}$, which we used in our calculations for the MM5-model, is provided by

$$\mathbf{n} = \mathbf{u}_h^{\perp}/|\mathbf{u}_h|, \tag{14}$$

where $\mathbf{u}_h = (u,v,0)^*$ is the horizontal component of the velocity, and $\mathbf{u}_h^{\perp} = (-v,u,0)^*$. In this case the binormal is given by

$$\mathbf{b} = \frac{1}{|\mathbf{u}||\mathbf{u}_h|}\left(-uw, -vw, |\mathbf{u}_h|^2\right)^*, \tag{15}$$

and the entries A_{ij} with $i > 1$ become

$$\begin{aligned} A_{12} &= \frac{1}{|\mathbf{u}||\mathbf{u}_h|}\Big\{(u^2-v^2)(u_y+v_x) + 2uv(v_y-u_x) \qquad + uw(v_z+w_y) - vw(u_z+w_x)\Big\}, \\ A_{13} &= \frac{1}{|\mathbf{u}|^2|\mathbf{u}_h|}\Big\{(|\mathbf{u}_h|^2-w^2)\big(v(v_z+w_y)+u(u_z+w_x)\big) - 2w(u^2u_x+v^2v_y) \\ &\quad -2uvw(u_y+v_x)\Big\}, \\ A_{22} &= \frac{1}{|\mathbf{u}_h|^2}\Big\{u^2v_y + v^2u_x - uv(u_y+v_x)\Big\}, \\ A_{23} &= \frac{|\mathbf{u}|\left(uv_z - vu_z\right)}{|\mathbf{u}_h|^2}, \\ A_{32} &= \frac{1}{|\mathbf{u}||\mathbf{u}_h|^2}\Big\{2w\big(v^2v_x - u^2u_y + uv(u_x-v_y)\big) + w^2(vu_z - uv_z) \\ &\quad +|\mathbf{u}_h|^2\big(uw_y - vw_x + w(u_y-v_x)\big)\Big\}, \\ A_{33} &= \frac{1}{|\mathbf{u}|^2|\mathbf{u}_h|^2}\Big\{w^2\big(u^2u_x+v^2v_y+uv(u_y+v_x)\big) \\ &\quad -|\mathbf{u}_h|^2w\big(u(u_z+w_x)+v(v_z+w_y)\big) + |\mathbf{u}_h|^4w_z\Big\}. \end{aligned}$$

3 Lagrangian fields

The Lagrangian fields display coherent sets of time-dependent structures, which can be visualized over varying initial times. The FTLE field shows many high regions of separation, including vortices and hyperbolic lines, while the Ψ_{22} field shows only hyperbolic separation, and the shearing is captured by the angle of rotation ϕ.

3.1 Structures and asymmetry

The LCS's are coherent through varying z-levels, showing the 3D nature of the structures, which indicates that vortex interaction plays a crucial role in the transport and organization of energy. Since the vortices reach heights of 10 km, well above the sea-surface, the role of WISHE in the transport of energy is seen as less important than the vortex interaction.

3.1.1 Initial crystalization phase

At 5 hours, the VHT's can be recognized as ringlike structures in the planar FTLE fields. Equivalent potential temperature (θ_e) contours indicate that the structures at this phase are highly localized and the Ψ_{22} ridges located between the vortex rings have the form of a "crystal lattice" with approximately hexagonal symmetry, that acts as a barrier to interaction between the vortices.

At 10 hours many VHT's are present in an annulus of about 60 to 80 km, seen as rings in the planar FTLE field, and as countours of high potential temperature. Filamentation has developed from the rings showing more interaction with neighboring VHT's. The filaments are also ridges of the Ψ_{22} field, which confirms that they are hyperbolic.

3.1.2 Eyewall formation

At 15 hours, the lattice structure has broken down (Figure 1), and by 20 hours (Figure 2), the number of mesovortices has been greatly reduced as many mergers and annihilations have occured. Triangular and square patterns formed by the dominant LCS's show that the remaining structural asymmetries are dominated by wavenumbers 3 and 4. Higher potential temperature air has entered into the core, and the breaks in the LCS lattice open pathways for the transport of material to the core. The fields between 20 and 30 hours initial times are shown in Figures 3 and 4.

Generally, the domain of influence of each mesovortex is determined by the length of the manifolds emanating from it. During the crystalization phase, the manifolds extend only to adjacent VHT's, and do not control any transport beyond the adjacent VHT's. By contrast, at 20 hours (Figure 2), the strength of the LCS's is much more intense, and some hyperbolic manifolds reach a length of over 50 km.

The structure of the VHT's in our 3D study is quite different from the 2D study of [15] and other studies in fluid mechanics, because of the lack of complete enclosure and presence of convection. In the 2D case, the vortex grows as it entrains additional fluid, and then splits a trailing shear layer of outflow from the vortex, often resulting in splitting into multiple vortices [14]. In the study of [15], the dominant vortex grows as it entrains the other vortex. For VHT interaction, we see that the size of VHT's generally grows as their entrainment of fluid increases. However, the open top of the VHT allows rising air to exit above $z = 10$ km, while there are two inflows present, at the sea surface and at $z = 6 - 9$ km [13, 10].

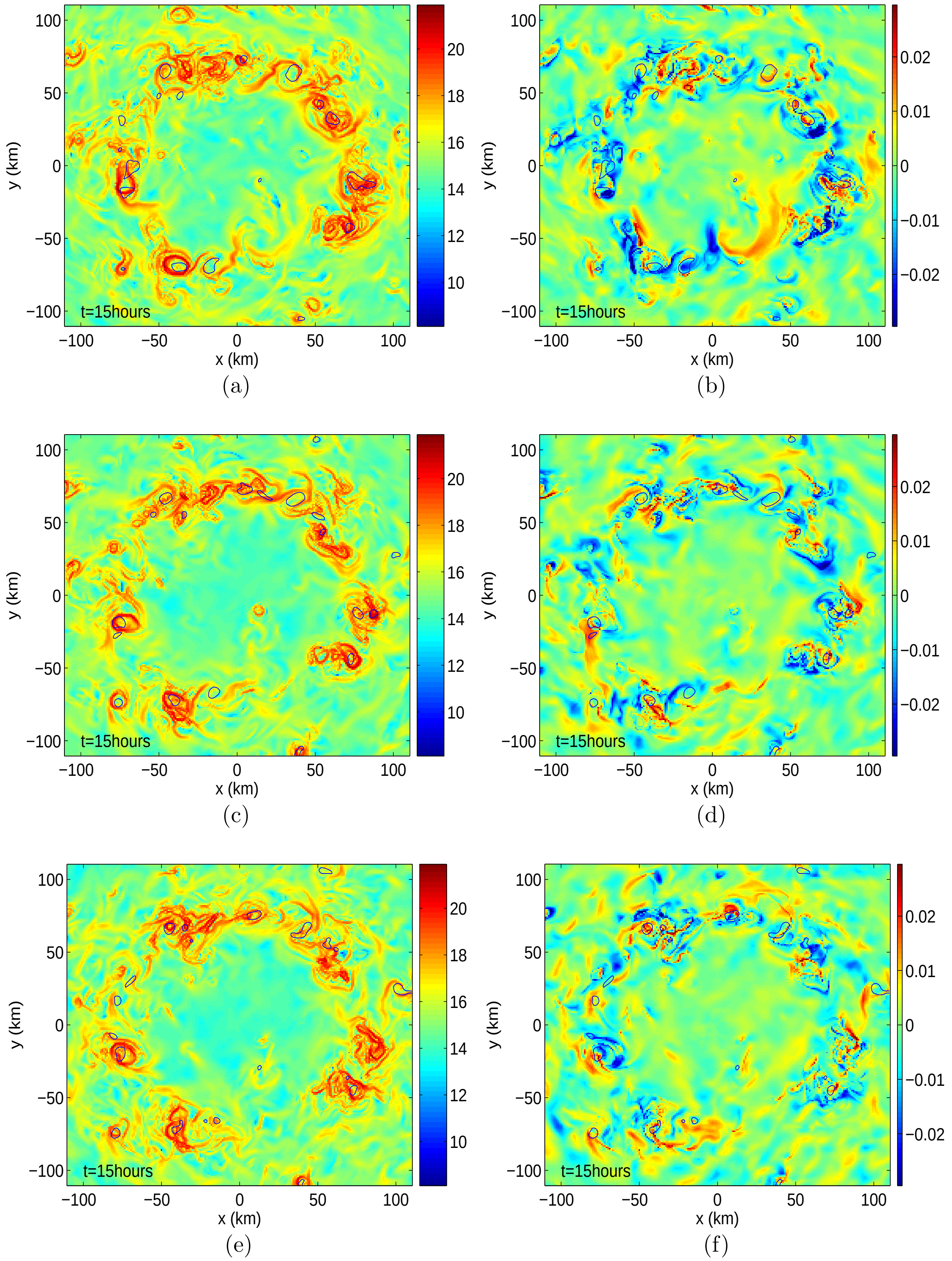

Figure 1: Planar FTLE fields (left column) and planar Ψ_{22} (right column) fields at z-levels of 1 km (a,b), 4 km (c,d), and 7 km (e,f) with 1 hour integration time and vorticity contours at initial time of 15 hours.

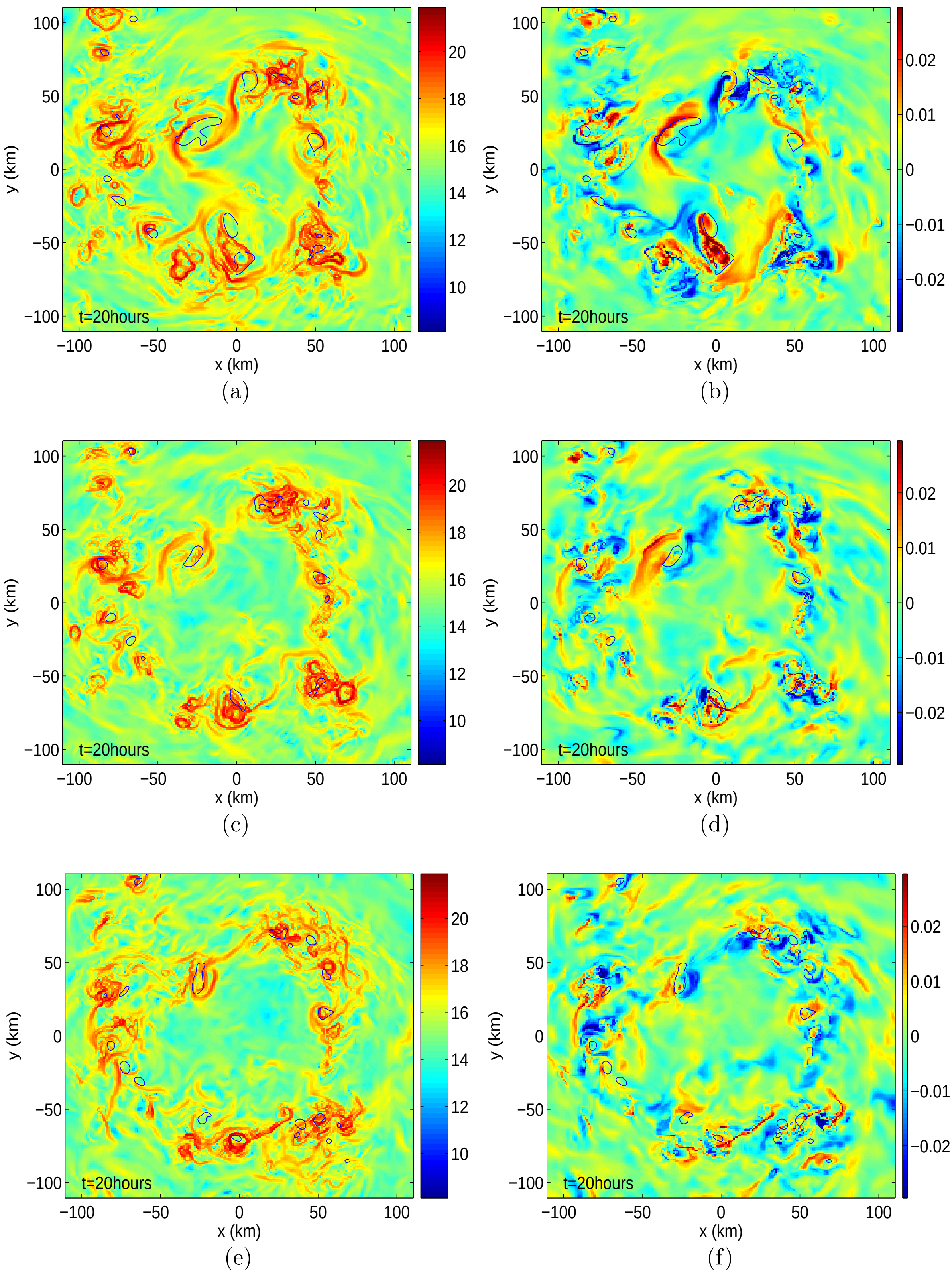

Figure 2: Planar FTLE fields (left column) and planar Ψ_{22} (right column) fields at z-levels of 1 km (a,b), 4 km (c,d), and 7 km (e,f) with 1 hour integration time and vorticity contours at initial time of 20 hours

3.2 Diabatic vortex merger

During the time period from 20 hours to 30 hours, several prominant vortices remain intact for longer than the normal 1 hour lifecycle and reach diameters of about 30 km. The merger of weaker vortices into the stronger vortex is illustrated in Figure 3, and can be clearly seen in an animation of the images.

A prominant vortex, labeled A in Figure 3 at 20 hours undergoes two types of mergers in the next 10 hour period. First, the vortex merges with smaller vortices that are located radially outward by a process of anihilation of the smaller vortices. The high vorticity in the outer vortices is filtered and contained within a tangle of manifolds. The outer vortices merge as the tangle unfolds into a single manifold at 24 hours. Merger of this new vortex with the inner vortex occurs at 26 hours when the manifolds unwind and release the vortex from its protective core in a pinchoff.

After the vortex has no manifold protecting it from interaction, it merges through a nearby tangle and becomes an elongated region of vorticity, which forms a portion of the eventual eyewall. The merger occurs first between 26 and 28 hours, and again between 28 and 30 hours. After the merger, the manifolds that protected the vortices have unwound and are located radially inward from the elongated vortex, now serving as a barrier to the center of the storm. The elongation and merger of primary VHT's is coincident with a higher rate of rotation. The VHT travels about one half rotation about the storm center for each 2 hour segment during the period from 20 to 26 hours, while it travels a full rotation during a 2 hour period from 28 hours to 30 hours, which indicates that an increase in angular velocity is a result of the upscale organization of vorticity through VHT interaction. Note that the length of the manifolds during the period of slower rotation is longer than the distance travelled by a trajectory during a 1 hour integration time, and that the coherent structures are far more resilliant than the 1 hour lifetimes of VHT's. The tight closure of manifolds around a VHT eliminates interaction, while the unwinding allows additional entrainment by the VHT, which is subsequently pinched off from the manifold.

References

[1] T. J. Dunkerton, M. T. Montgomery, and Z. Wang. Tropical cyclogenesis in a tropical wave critical layer: easterly waves. *Atmos. Chem. Phys.*, 9:5587–5646, 2009.

[2] W. M. Frank and E. A. Ritchie. Effects of environmental flow upon tropical cyclone structure. *Mon. Wea. Rev.*, 127:2044–2061, 1999.

[3] W. M. Frank and E. A. Ritchie. Effects of vertical wind shear on the intensity and structure of numerically simulated hurricanes. *Mon. Wea. Rev.*, 129:2249–2269, 2001.

[4] J. J. Hack and W. H. Schubert. Nonlinear response of atmospheric vortices to heating by organized cumulus convection. *J. Atmos. Sci.*, 43:1559–1573, 1986.

[5] G. Haller. Finding finite-time invariant manifolds in two-dimensional velocity fields. *Chaos*, 10:99–108, 2000.

[6] G. Haller. Lagrangian coherent structures from approximate velocity data. *Physics of Fluids*, 14:1851–1861, 2002.

[7] G. Haller and R. Iacono. Stretching, alignment, and shear in slowly varying velocity fields. *Physical Review E*, 68:056304–1–6, 2003.

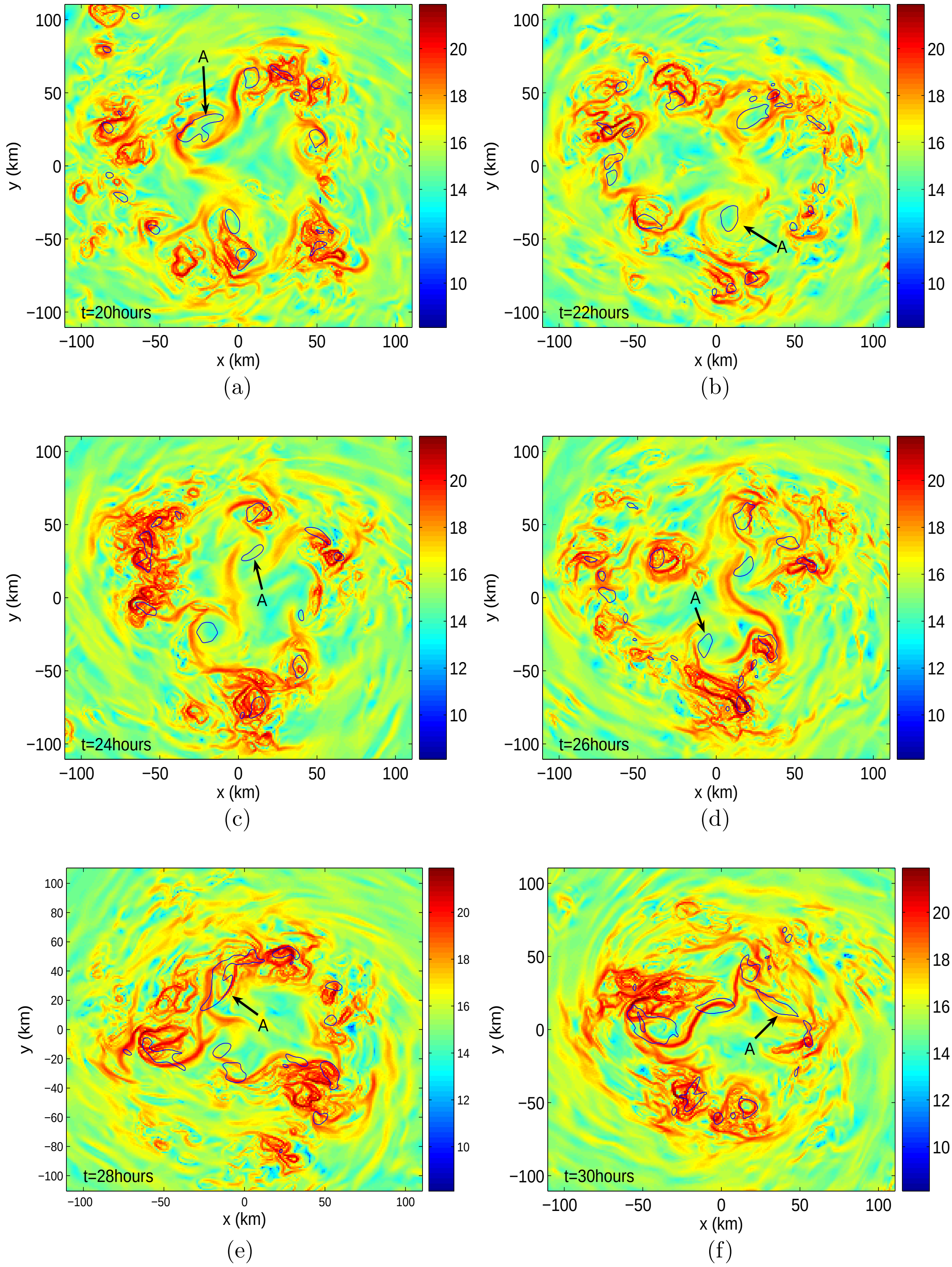

Figure 3: Planar FTLE fields with 1 hour integration time and vorticity contours at times from 20 hours to 30 hours every 2 hours.

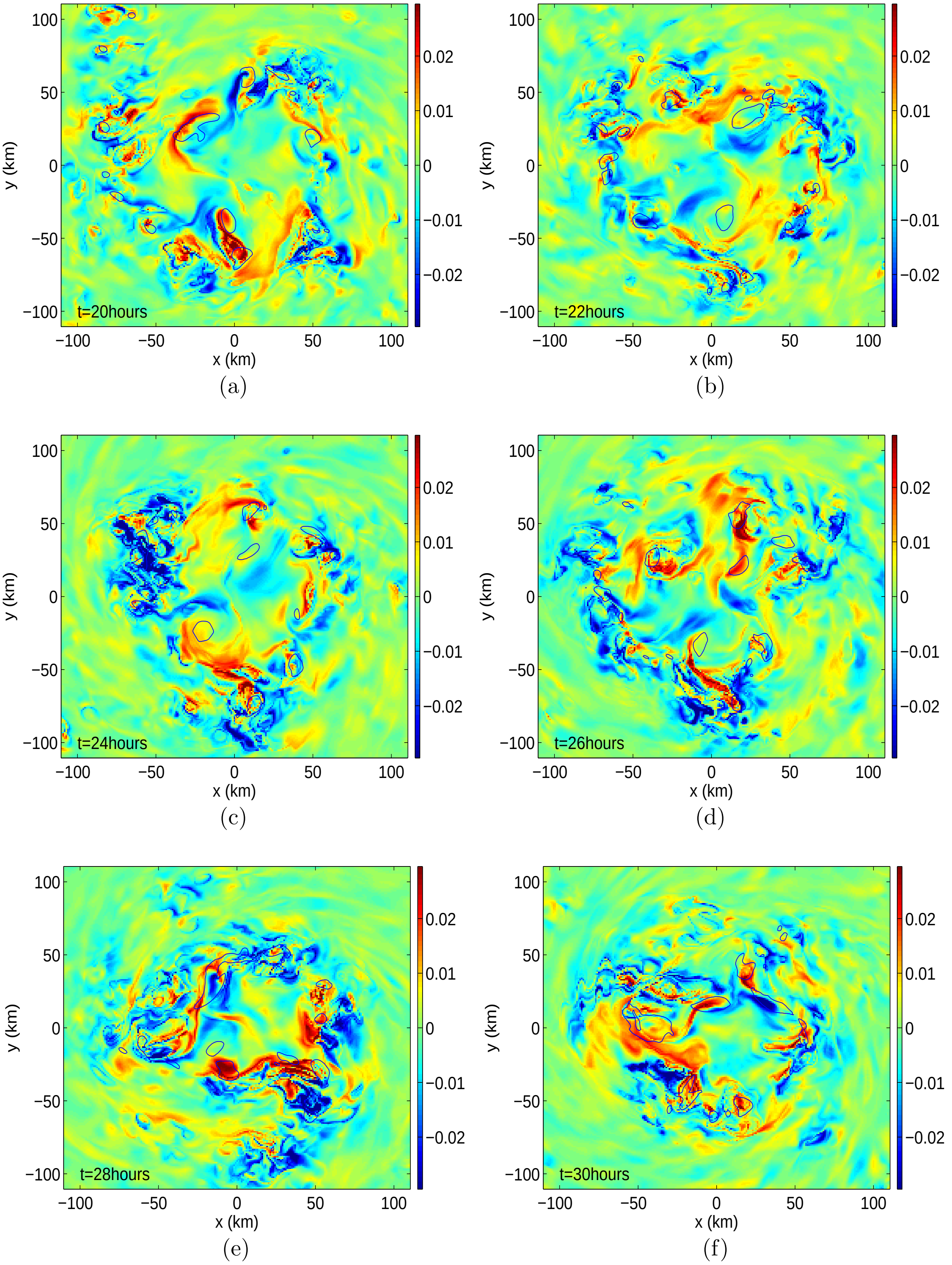

Figure 4: Planar $\Psi_2 2$ fields with 1 hour integration time and vorticity contours at times from 20 hours to 30 hours every 2 hours.

[8] G. Haller and A. Poje. Finite time transport in aperiodic flows. *Physica D*, 119:352–380, 1997.

[9] G. Haller and G. Yuan. Lagrangian coherent structures and mixing in two-dimensional turbulence. *Physica D*, 147:352–370, 2000.

[10] E. A. Hendricks, M. T. Montgomery, and C. A. Davis. On the role of vortical hot towers in tropical cyclone formation. *J. Atmos. Sci.*, 61:1209–1232, 2004.

[11] J. C. McWilliams. The emergence of isolated coherent vortices in turbulent flow. *J. Fluid Mech.*, 140:21–43, 1984.

[12] M. T. Montgomery, V. S. Nguyen, R. K. Smith, and J. Persing. Do tropical cyclones intensify by wishe? *Q. J. R. Meteorol. Soc.*, 135:1697–1714, 2009.

[13] M. T. Montgomery, M. E. Nichols, T. A. Cram, and A. B. Saunders. A vortical hot tower route to tropical cyclogenesis. *J. Atmos. Sci.*, 63:355–386, 2006.

[14] C. O'Farrell and J. O. Dabiri. A lagrangian approach to identifying vortex pinch-off. *Chaos*, 20:017513–1–9, 2010.

[15] R. Prieto, B.D. McNoldy, S.R. Fulton, and W.H. Schubert. A classification of binary tropical-cyclone-like vortex interactions. *Mon. Wea.Rev.*, 131:2656–2666, 2003.

[16] B. Rutherford, G. Dangelmayr, J. Persing, , M. Kirby, and M. T. Montgomery. A 3d lagrangian hurricane eye-eyewall computation. Preprint, submitted to Quart. J. Roy. Met. Soc., 2009.

[17] B. Rutherford, G. Dangelmayr, J. Persing, W. H. Schubert, and M. T. Montgomery. Advective mixing in a nondivergent barotropic hurricane model. *Atmos. Chem. Phys.*, 10:475–497, 2010.

[18] W. H. Schubert and J. J. Hack. Inertial stability and tropical cyclone development. *J. Atmos. Sci.*, 39:1687–1697, 1982.

[19] S. C. Shadden, F. Lekien, and J. E. Marsden. Definition and properties of lagrangian coherent structures from finite-time lyapunov exponents in two-dimensional aperiodic flows. *Physica D*, 212:271–304, 2005.

[20] R. K. Smith, M. T. Montgomery, and V. S. Nguyen. Tropical cyclone spin up revisited. *Q. J. R. Meteorol. Soc.*, 134:1385–1395, 2009.